DTU Library

Highly sensitive and simple method for refractive index sensing of liquids in microstructured optical fibers using four-wave mixing

Frosz, Michael Henoch; Stefani, Alessio; Bang, Ole

[Link back to DTU Orbit](#)

Highly sensitive and simple method for refractive index sensing of liquids in microstructured optical fibers using four-wave mixing

Michael H. Frosz, Alessio Stefani, and Ole Bang*

DTU Fotonik, Department of Photonics Engineering, Technical University of Denmark,
Ørsteds Plads 343,
DK-2800 Kgs. Lyngby, Denmark
*[*oban@fotonik.dtu.dk](mailto:oban@fotonik.dtu.dk)*

Abstract: We present both experimental measurements and simulations for a simple fiber-optical liquid refractive index sensor, made using only commercially available components and without advanced postprocessing of the fiber. Despite the simplicity, we obtain the highest sensitivity experimentally demonstrated to date for aqueous solutions (refractive index around 1.33), which is relevant for extensions to biosensing. The sensor is based on measuring the spectral shift of peaks arising from four-wave mixing (FWM), when filling the holes of a microstructured fiber with different liquid samples and propagating nanosecond pulses through the silica-core of the fiber. To the best of our knowledge, this is also the first experiment where a liquid is filled into the holes of a solid-core microstructured fiber to control the phase-match conditions for FWM.

© 2011 Optical Society of America

OCIS codes: (060.4005) Microstructured fibers; (060.4370) Nonlinear optics, fibers; (060.5295) Photonic crystal fibers; (190.4370) Nonlinear optics, fibers; (190.4380) Nonlinear optics, four-wave mixing.

References and links

1. M. E. Bosch, A. J. R. Sánchez, F. S. Rojas, and C. B. Ojeda, "Recent development in optical fiber biosensors," Sensors **7**, 797–859 (2007).
2. X. Fan, I. M. White, S. I. Shopova, H. Zhu, J. D. Suter, and Y. Sun, "Sensitive optical biosensors for unlabeled targets: a review," Anal. Chim. Acta **620**, 8–26 (2008).
3. P. E. Hoiby, L. B. Nielsen, J. B. Jensen, T. P. Hansen, A. Bjarklev, and L. H. Pedersen, "Molecular immobilization and detection in a photonic crystal fiber," (SPIE, 2004), vol. 5317, pp. 220–223. http://dx.doi.org/10.1117/12.528891.
4. J. B. Jensen, P. E. Hoiby, G. Emiliyanov, O. Bang, L. Pedersen, and A. Bjarklev, "Selective detection of antibodies in microstructured polymer optical fibers," Opt. Express **13**, 5883–5889 (2005).
5. L. Rindorf, J. B. Jensen, M. Dufva, L. H. Pedersen, P. E. Høiby, and O. Bang, "Photonic crystal fiber long-period gratings for biochemical sensing," Opt. Express **14**, 8224–8231 (2006).
6. J. E. Sharping, M. Fiorentino, A. Coker, P. Kumar, and R. S. Windeler, "Four-wave mixing in microstructure fiber," Opt. Lett. **26**, 1048–1050 (2001).
7. J. D. Harvey, R. Leonhardt, S. Coen, G. K. L. Wong, J. C. Knight, W. J. Wadsworth, and P. St. J. Russell, "Scalar modulation instability in the normal dispersion regime by use of a photonic crystal fiber," Opt. Lett. **28**, 2225–2227 (2003).
8. M. H. Frosz, T. Sørensen, and O. Bang, "Nanoengineering of photonic crystal fibers for supercontinuum spectral shaping," J. Opt. Soc. Am. B **23**, 1692–1699 (2006).

9. J. R. Ott, M. Heuck, C. Agger, P. D. Rasmussen, and O. Bang, "Label-free and selective nonlinear fiber-optical biosensing," Opt. Express **16**, 20834–20847 (2008).

10. N. I. Nikolov, T. Sørensen, O. Bang, and A. Bjarklev, "Improving efficiency of supercontinuum generation in photonic crystal fibers by direct degenerate four-wave mixing," J. Opt. Soc. Am. B **20**, 2329–2337 (2003).

11. J. M. Fini, "Microstructure fibres for optical sensing in gases and liquids," Meas. Sci. Technol. **15**, 1120–1128 (2004).

12. S. O. Konorov, A. B. Fedotov, A. M. Zheltikov, and R. B. Miles, "Phase-matched four-wave mixing and sensing of water molecules by coherent anti-Stokes Raman scattering in large-core-area hollow photonic-crystal fibers," J. Opt. Soc. Am. B **22**, 2049–2053 (2005).

13. P. D. Rasmussen, F. H. Bennet, D. N. Neshev, A. A. Sukhorukov, C. R. Rosberg, W. Krolikowski, O. Bang, and Y. S. Kivshar, "Observation of two-dimensional nonlocal gap solitons," Opt. Lett. **34**, 295–297 (2009).

14. G. P. Agrawal, *Nonlinear Fiber Optics* 4th ed. (Academic Press, 2007).

15. V. Tombelaine, A. Labruyère, J. Kobelke, K. Schuster, V. Reichel, P. Leproux, V. Couderc, R. Jamier, and H. Bartelt, "Nonlinear photonic crystal fiber with a structured multi-component glass core for four-wave mixing and supercontinuum generation," Opt. Express **17**, 15392–15401 (2009).

16. N. A. Mortensen, J. R. Folkenberg, M. D. Nielsen, and K. P. Hansen, "Modal cutoff and the V parameter in photonic crystal fibers," Opt. Lett. **28**, 1879–1881 (2003).

17. S. G. Johnson and J. D. Joannopoulos, "Block-iterative frequency-domain methods for Maxwell's equations in a planewave basis," Opt. Express **8**, 173–190 (2001).

18. J. Lægsgaard, A. Bjarklev, and S. E. B. Libori, "Chromatic dispersion in photonic crystal fibers: fast and accurate scheme for calculation," J. Opt. Soc. Am. B **20**, 443–448 (2003).

19. D. N. Nikogosyan, *Properties of optical and laser-related materials: a handbook* (John Wiley & Sons Ltd., West Sussex, England, 1997).

20. J. E. Bertie and Z. Lan, "The refractive index of colorless liquids in the visible and infrared: Contributions from the absorption of infrared and ultraviolet radiation and the electronic molar polarizability below 20 500 cm^{-1}," J. Chem. Phys. **103**, 10152–10161 (1995). `http://link.aip.org/link/?JCP/103/10152/1`.

21. J. E. Bertie and Z. Lan, "Infrared intensities of liquids XX: The intensity of the OH stretching band of liquid water revisited, and the best current values of the optical constants of $H_2O(l)$ at 25°C between 15,000 and 1 cm^{-1}," Appl. Spectrosc. **50**, 1047–1057 (1996). `http://as.osa.org/abstract.cfm?URI=as-50-8-1047`.

22. The International Association for the Properties of Water and Steam, "Release on the refractive index of ordinary water substance as a function of wavelength, temperature and pressure," (1997). `http://www.iapws.org/relguide/rindex.pdf`.

23. J. E. Bertie, S. L. Zhang, H. H. Eysel, S. Baluja, and M. K. Ahmed, "Infrared intensities of liquids XI: Infrared refractive indices from 8000 to 2 cm^{-1}, absolute integrated intensities, and dipole moment derivatives of methanol at 25°C," Appl. Spectrosc. **47**, 1100–1114 (1993).

24. S. E. Wood, S. Langer, and R. Battino, "Refractive index and dispersion of the benzene-methanol system," J. Chem. Phys. **32**, 1389–1393 (1960). `http://link.aip.org/link/?JCP/32/1389/1`.

25. M. H. Frosz, "Dispersion-modulation by high material loss in microstructured polymer optical fibers," Opt. Express **17**, 17950–17962 (2009).

26. K. Okamoto, *Fundamentals of Optical Waveguides* 2nd ed. (Academic Press, 2006).

27. I. H. Malitson, "Interspecimen comparison of the refractive index of fused silica," J. Opt. Soc. Am. **55**, 1205–1209 (1965).

28. J. M. Dudley, G. Genty, and S. Coen, "Supercontinuum generation in photonic crystal fiber," Rev. Mod. Phys. **78**, 1135–1184 (2006). `http://link.aps.org/abstract/RMP/v78/p1135`.

29. J. C. Travers, M. H. Frosz, and J. M. Dudley, *Nonlinear Fibre Optics Overview* (Cambridge University Press, 2010), chap. 3, Supercontinuum generation in optical fibers. ISBN 978-0-521-51480-4.

30. J. Lægsgaard, "Mode profile dispersion in the generalised nonlinear Schrödinger equation," Opt. Express **15**, 16110–16123 (2007).

31. K. J. Blow and D. Wood, "Theoretical description of transient stimulated Raman scattering in optical fibers," IEEE J. Quantum Electron. **25**, 2665–2673 (1989).

32. M. H. Frosz, P. M. Moselund, P. D. Rasmussen, C. L. Thomsen, and O. Bang, "Increasing the blue-shift of a supercontinuum by modifying the fiber glass composition," Opt. Express **16**, 21076–21086 (2008).

33. P. D. Rasmussen, J. Lægsgaard, and O. Bang, "Degenerate four wave mixing in solid core photonic bandgap fibers," Opt. Express **16**, 4059–4068 (2008).

34. J. Hult, "A fourth-order Runge–Kutta in the interaction picture method for simulating supercontinuum generation in optical fibers," J. Lightwave Technol. **25**, 3770–3775 (2007).

35. M. H. Frosz, "Validation of input-noise model for simulations of supercontinuum generation and rogue waves," Opt. Express **18**, 14778–14787 (2010).

36. S. Coen, A. H. L. Chau, R. Leonhardt, J. D. Harvey, J. C. Knight, W. J. Wadsworth, and P. St. J. Russell, "Supercontinuum generation by stimulated Raman scattering and parametric four-wave mixing in photonic crystal fibers," J. Opt. Soc. Am. B **19**, 753–764 (2002).

37. H. R. Zelsmann, "Temperature dependence of the optical constants for liquid H_2O and D_2O in the far IR region,"

      J. Mol. Struct. **350**, 95–114 (1995).

38. J. F. Mammone, S. K. Sharma, and M. Nicol, "Raman spectra of methanol and ethanol at pressures up to 100 kbar," J. Phys. Chem. **84**, 3130–3134 (1980).
39. L. Rindorf and O. Bang, "Highly sensitive refractometer with a photonic-crystal-fiber long-period grating," Opt. Lett. **33**, 563–565 (2008). http://ol.osa.org/abstract.cfm?URI=ol-33-6-563.
40. D. K. C. Wu, B. T. Kuhlmey, and B. J. Eggleton, "Ultrasensitive photonic crystal fiber refractive index sensor," Opt. Lett. **34**, 322–324 (2009).
41. B. T. Kuhlmey, S. Coen, and S. Mahmoodian, "Coated photonic bandgap fibres for low-index sensing applications: cutoff analysis," Opt. Express **17**, 16306–16321 (2009).
42. W. Yuan, G. E. Town, and O. Bang, "Refractive index sensing in an all-solid twin-core photonic bandgap fiber," IEEE Sensors J. **10**, 1192–1199 (2010).

1. Introduction

Fiber-optical biosensors typically rely on either detecting a change in some linear property of the optical fiber, such as the shift in a resonance (grating, surface plasmon, two-core coupling, Fabry-Perot, etc.), or on detecting the appearance of fluorescence caused by the presence of the biomolecules searched for [1, 2]. One fluorescence-based method involves microstructured optical fibers (MOFs) chemically treated to have a capture layer on the inside of the air-holes running along the MOF [3,4]. When a liquid sample is introduced into the air-holes, the capture layer highly selectively bonds (e.g. antigen-antibody bonding) with matching bio-molecules in the sample. By beforehand labeling the bio-molecules with fluorophores, one can detect the fluorescence occurring from the thin ($\sim$5–10 nm) layer of fluorophores captured on the inside of the holes. In one example of a label-free method one measures the shift in a long-period grating resonance caused by the capture of bio-molecules inside the holes of the MOF [5].

MOFs have also received a great deal of attention for their usefulness as a nonlinear optical medium in generating new spectral components through effects such as four-wave mixing (FWM) [6, 7]. Interestingly, it was found that the spectral location of the FWM-peaks can shift significantly when varying the air-hole size by just $\sim$10 nm, due to the extreme sensitivity of FWM to the dispersion profile of the MOF [8]. This recently led to the idea of label-free biosensing by instead exploiting the inherent nonlinearity of MOFs [9]. In this novel approach, the capture layer is added to the MOF air-holes in the same way as demonstrated previously for fluorescence detection [3, 4]. However, the liquid sample is then introduced into the air-holes without any fluorophore labeling of the sample, thereby simplifying the procedure. Instead, intense pump pulses are coupled into the MOF and the output spectrum is measured with an optical spectrum analyzer (OSA). Apart from the residual pump spectrum, the output spectrum contains two newly generated peaks from FWM. If the sample contains the biomolecules matching the capture layer, the inner diameter of the air-holes will effectively have decreased thereby slightly changing the dispersion of the MOF, and shifting the spectral location of the FWM peaks. Detecting the location of the FWM peaks using an OSA then reveals whether the biomolecules are present in the sample or not.

The work by Ott *et al.* showed theoretically that the principle can be used to sense a 5 nm thick layer of biomolecules by detecting a 26 nm shift in the FWM anti-Stokes-peak [9]. However, it remained to be determined whether this would be detectable in practice, or whether the unavoidable fabrication fluctuations in the microstructure along the MOF length would decrease the effective FWM gain too much for the FWM peak to be detected. Fluctuations in the microstructure can be expected to be particularly detrimental for FWM pumped in the normal dispersion regime, because of the very narrow gain regions in this pumping regime [7, 8, 10]. In this work we therefore experimentally demonstrate that it is possible to fill the air-holes of a MOF with liquids (water and methanol) and still detect the location of the anti-Stokes peak. The principle relies on a simple experimental setup where all components are commercially available, requiring no special fibers or complicated postprocessing of the optical fiber. We

show that the principle can also be used to measure refractive index changes of the liquid in the holes, and demonstrate a shift in the anti-Stokes peak of 28 nm for a change in refractive index units of 0.003 at the pump wavelength (1064 nm). Measuring small refractive index changes of aqueous solutions has received a lot of attention recently because the refractive index change can be used to reveal the presence of specific biomolecules in a sample. We also calculate the location of the anti-Stokes peaks theoretically and find good agreement with the experiments.

We should also point out that both linear and nonlinear experiments with liquids in MOFs usually involves propagating the pump light in a liquid-filled core to ensure a high overlap between the light and the liquid [11–13]. Our experiments, on the other hand, rely on propagating the pump in a silica core while detecting subtle changes in the effective index of the waveguide caused by the liquid in the holes *surrounding* the core. It is therefore not necessary for the liquid to be highly nonlinear, since the principle relies only on the linear optical properties of the liquid. We show that differentiation between two liquids is possible despite the low overlap between the pump light and the liquid. It is also the first time, to the best of our knowledge, that filling a liquid into the holes of a solid-core MOF is used experimentally to control the phase-match conditions for FWM.

2. Theory

2.1. Four-wave mixing for refractive index sensing

Degenerate four-wave mixing (FWM) can be viewed [14] as the simultaneous annihilation of two pump photons at angular frequency ω_p and creation of two new photons, where one is down-shifted (Stokes-shifted) to ω_S and the other is up-shifted (anti-Stokes-shifted) to ω_{aS}. It follows from energy-conservation that $2\omega_p = \omega_{aS} + \omega_S$. For the process to be efficient, the phase-mismatch κ,

$$\kappa = 2\beta(\omega_p) - \beta(\omega_S) - \beta(\omega_{aS}) - 2\gamma P_0, \tag{1}$$

must fulfill [14]:

$$|\kappa| < 2\gamma P_0, \tag{2}$$

where $\beta(\omega)$ is the propagation constant of the waveguide at frequency ω; it can also be expressed as $n_{eff}2\pi/\lambda$, where n_{eff} is the effective index of the waveguide. γ is the nonlinear parameter given by $\gamma = n_2\omega_p/(cA_{eff})$, where $n_2 = 2.6 \cdot 10^{-20}$ m^2/W is the nonlinear-index coefficient for silica, c is the speed of light in vacuum, and A_{eff} is the effective core area [14]; it is assumed in the equations for κ above that the frequency variation of A_{eff} is sufficiently small to consider γ practically constant over the relevant frequency range. P_0 is the peak power of the pump in the waveguide. Note that basing the sensor on the FWM-process with the phase-match condition given in Eq. (1), means that one is actually probing the liquid at *three* widely separated frequencies simultaneously, ω_p, ω_S, and ω_{aS}, using just *one* pump frequency. The wide frequency separation between ω_S and ω_{aS} occurring when pumping in the normal dispersion regime, will be apparent in the following.

For highest sensitivity (defined as shift in ω_S and ω_{aS} when changing the refractive index of the liquid) one should choose the structure of the MOF such that the zero-dispersion wavelength (ZDW) is close to the pump wavelength, when the MOF is filled with the liquid [9]. We here choose a pump at 1064 nm due to the availability of compact, rugged and relatively low-cost microchip lasers at this wavelength. However, as shown in Fig. 8 of Ref. [9], it is not possible to obtain a ZDW at 1064 nm in a water-filled MOF unless the relative air-hole diameter $d/\Lambda \gtrsim 0.7$. Such a high d/Λ unfortunately leads to a highly-multimoded fiber, which would allow the generation of more sets of phase-matched Stokes and anti-Stokes peaks in the output spectrum
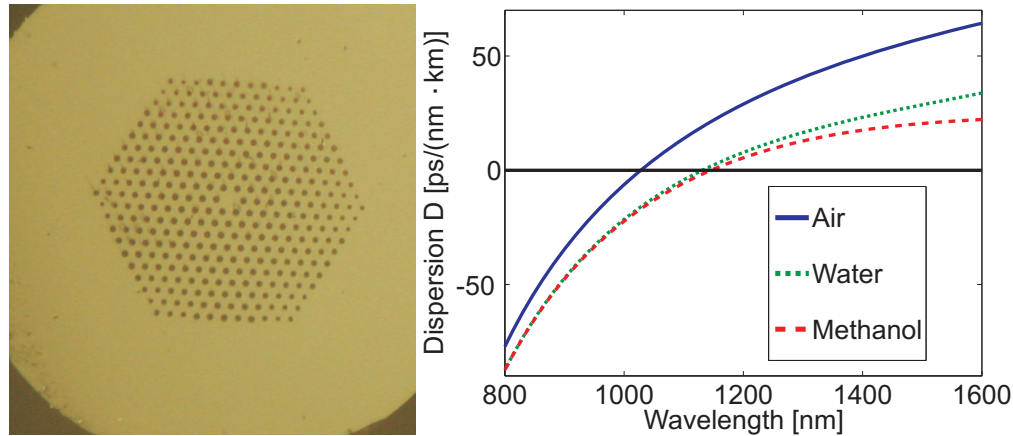
Fig. 1. *Left:* Microscope image showing the cross-section of the photonic crystal fiber used here. The distance between air-holes is $\Lambda = 3.15$ μm, and the relative hole diameter is $d/\Lambda = 0.5$. *Right:* Calculated dispersion profiles for the MOF-waveguide when the holes are either filled with air (blue, solid), water (green, dotted), or methanol (red, dashed). The horizontal black line indicates zero dispersion.

[15]. This could complicate the interpretation of the output spectrum. Filling the holes with a liquid is expected to make it less multimoded, due to the smaller refractive index contrast [16], but to be certain that the fiber was single-moded even for the experiments with only air in the holes, we compromised for a highly-nonlinear MOF with a smaller d/Λ: the NL-4.7-1030 (NKT Photonics A/S, Birkerød, Denmark). This fiber has a pitch of $\Lambda = 3.15$ μm, $d/\Lambda = 0.5$; when there is only air in the holes it has a single-mode cutoff at 1024 nm (so it is single-moded at the pump wavelength) and a ZDW of ∼1030 nm. An image of the MOF cross-section is shown in Fig. 1, left.

   Using the freely available MPB-software [17] together with a self-consistent scheme to include material dispersion $n(\lambda)$ [18] to calculate $\beta(\omega)$, we found that the ZDW is shifted to ∼1130 nm when the MOF-holes are filled with water (Fig. 1, right) which is relevant for aqueous solutions with biomolecules. As described in Ref. [9] one can attach a layer of capture-molecules on the inside of the MOF-holes, so that only a specifically matching type of biomolecules in the probed sample are captured on the inside of the holes. The capture of the targeted biomolecules in the sample leads to a change in the effective index of the waveguide, which shifts the FWM-generated peaks, thereby revealing the presence of the targeted biomolecules in the sample. To demonstrate the shift in FWM-peaks experimentally, we chose to fill the fiber with either water (so that the refractive index is close to that of aqueous solutions in general) or methanol. Using water and methanol instead of aqueous solutions with biomolecules allows us to use refractive index data available in the literature over a wide frequency range, so that a clearer comparison between calculations and experiments can be made for validation. Also, methanol has a refractive index of $n \sim 1.32$ at 1064 nm, so it is close to that of water ($n \sim 1.32$). Other colorless liquids available in chemically very pure form and with well-characterized optical properties, that could potentially have been used for this investigation, unfortunately have significantly higher refractive index; e.g., at 656 nm ethanol has $n \sim 1.36$, acetone has $n \sim 1.36$, and benzene has $n \sim 1.50$ [19]. For a comparison at the same wavelength, water has $n \sim 1.33$ and methanol has $n \sim 1.33$ at 656 nm [19]. We found that the higher refractive index for e.g. acetone causes the estimated Stokes-peak to shift so far into the infrared (∼ 3450 nm) that losses cannot be neglected, and reliable refractive index data are not

available, so extrapolation far beyond the available data would be required; therefore the estimation of both the Stokes and anti-Stokes peak location becomes very uncertain. Also, if the refractive index of the liquid is chosen too close to that of the silica glass ($n \sim 1.45$) one has the additional disadvantage of poorer confinement in the MOF core, due to the reduced refractive index contrast.

2.2. Obtaining refractive index data over the broad wavelength range considered

To predict the location of the FWM-peaks it is necessary to have reliable refractive index data for the liquids (and the silica glass) both in the visible and the near-infrared; note that even though the peak at ω_{aS} is found to be located in the visible, one also needs to know the refractive index in the near-infrared (where ω_S is found to be located) to make predictions for ω_{aS} and ω_S using Eq. (1). The refractive index data for water are therefore obtained from the expression found in [20] using some additional terms:

$$n(\tilde{v}) \approx a_0 + a_2 \tilde{v}^2 + a_4 \tilde{v}^4 - \frac{a_{-2}}{\tilde{v}^2} - \frac{a_{-4}}{\tilde{v}^4} - \frac{a_{-6}}{\tilde{v}^6} - \frac{a_{-8}}{\tilde{v}^8} - \frac{a_{-10}}{\tilde{v}^{10}} - \frac{a_{-12}}{\tilde{v}^{12}}, \tag{3}$$

where $\tilde{v}$ is the wavenumber in units of cm^{-1}. The first four coefficients we used are the same as in Ref. [20], while the last five coefficients were obtained by fitting to refractive index data between 667 nm and 2.4 µm from Table III in Ref. [21]. The resulting fit was found to be accurate within ± 0.002 ($\sim 0.2\%$) between 667 nm–2.4 µm compared to the data from Table III in Ref. [21], and within ± 0.00086 ($\sim 0.06\%$) in the wavelength range 300–1100 nm when comparing to IAPWS data [22] at a temperature of 298.15 K and a density of 997 kg/m^3. The used fitting coefficients for water are: $a_0 = 1.326652$, $a_2 = 24.5610 \cdot 10^{-12}$ cm^2, $a_4 = 3.4713 \cdot 10^{-21}$ cm^4, $a_{-2} = 43.2 \cdot 10^4$ cm^{-2}, $a_{-4} = 3.8530 \cdot 10^{12}$ cm^{-4}, $a_{-6} = 3.8036 \cdot 10^{19}$ cm^{-6}, $a_{-8} = 1.2340 \cdot 10^{26}$ cm^{-8}, $a_{-10} = 1.5904 \cdot 10^{32}$ cm^{-10}, and $a_{-12} = 2.2029 \cdot 10^{41}$ cm^{-12}.

The refractive index data for methanol were calculated from

$$n^2(\tilde{v}) \approx b_0 + b_2 \tilde{v}^2 + b_4 \tilde{v}^4 + c_0 \frac{\tilde{v}_0^2(\tilde{v}_0^2 - \tilde{v}^2)}{(\tilde{v}_0^2 - \tilde{v}^2)^2 + (\tilde{v}\Delta\tilde{v})^2} \tag{4}$$

where b_0, b_2, and b_4 are again found in Ref. [20]. The additional coefficients c_0, $\tilde{v}_0$, and $\Delta\tilde{v}$ were found by fitting to data between 1.25 µm and 2.9 µm from Table III in Ref. [23] (these data were first corrected to higher accuracy by using Eq. (7) in Ref. [20]). The resulting fit was found to agree to within $\pm 4 \cdot 10^{-4}$ ($\sim 0.03\%$) for data from Table I in Ref. [24] (405–656 nm) and to within ± 0.002 ($\sim 0.2\%$) for the (corrected) data from Table III in Ref. [23] (1.25–2.9 µm). The used fitting coefficients for methanol are: $b_0 = 1.740918$, $b_2 = 58.891 \cdot 10^{-12}$ cm^2, $b_4 = 22.11 \cdot 10^{-21}$ cm^4, $c_0 = 0.021805$, $\tilde{v}_0 = 3407$ cm^{-1}, and $\Delta\tilde{v} = 158.2$ cm^{-1}. It was necessary to add the last term in Eq. (4) because of an absorption peak centered around 3342 cm^{-1} (2.99 µm) [23], which causes a strong drop in the real part of n from ~ 2.4 µm to 2.87 µm, followed by a sharp increase in n. Since we find, both experimentally and from the calculations, that the FWM Stokes peak with methanol in the holes is located at 2.6 µm, we assume that we do not need reliable data for n above 2.9 µm; also it seems reasonable to neglect the imaginary part of n when calculating $\beta(\lambda)$ for the waveguide, as long as $\beta(\lambda)$ does not need to be calculated too close to the absorption peak at 2.99 µm. We note that pumping close to an absorption peak causes a shift in the FWM peaks, because the Kramers-Kronig relation links together dispersion modulation and absorption [25].

The refractive index of silica was found using the Sellmeier expression (p. 92 in Ref. [26])

$$n^2 = 1 + \frac{0.6965325\lambda^2}{\lambda^2 - (0.066093)^2} + \frac{0.4083099\lambda^2}{\lambda^2 - (0.11811001)^2} + \frac{0.8968766\lambda^2}{\lambda^2 - (9.896160)^2}, \tag{5}$$
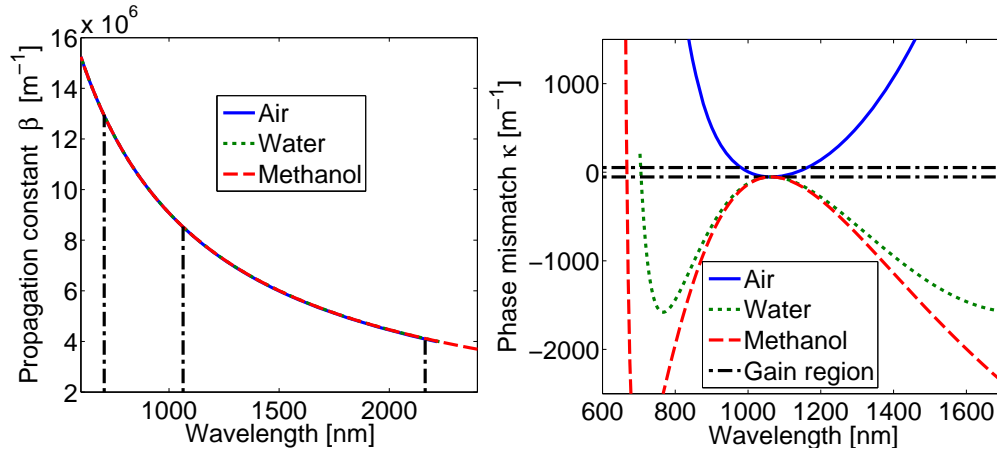
Fig. 2. *Left:* Calculated propagation constant for the used MOF with either air (blue, solid), water (green, dotted), or methanol (red, dashed) in the holes. The dash-dotted vertical lines indicate (from left to right) the anti-Stokes, pump, and Stokes wavelength, respectively, for the case of water in the holes. *Right:* The calculated phase-mismatch κ, Eq. (1), with either air (blue, solid), water (green, dotted), or methanol (red, dashed) in the holes. The horizontal dash-dotted lines indicate the limits of the gain region, Eq. (2).

with the wavelength λ in μm, and is found to deviate less than $\sim 3 \cdot 10^{-4}$ ($\sim 0.02\%$) from refractive index measurements of fused silica in the range 300–3700 nm [27].

2.3. Phase-matching calculations

In Fig. 2, left, we show the calculated propagation constant $\beta(\lambda)$ over the wavelength range of interest, when there is either air, water, or methanol in the holes of the MOF-waveguide. The first thing to notice is that the difference in β between the three considered cases is too small to be seen on the used scale. Therefore, one could initially think that the change in waveguide dispersion caused by inserting liquid into the holes is too small to be detected, and that it would be even more difficult to distinguish between two different liquids. The change in β is so small mostly because only a small fraction of the propagating light extends into the holes to interact with the liquids. This is in sharp contrast to the work using a hollow-core MOF filled with a liquid, where a high overlap between the light and the liquid is assured [12]. However, it turns out that the extremely high $\beta(\lambda)$ sensitivity of the FWM-process, as expressed by Eqs. (1)–(2), leads to a clear difference in the theoretically expected FWM-peaks.

The high sensitivity to small differences in β is seen clearly in Fig. 2, right, where we have calculated the phase-mismatch κ according to Eq. (1), using $\gamma = 0.012 \ (\mathrm{W} \cdot \mathrm{m})^{-1}$ and $P_0 = 2.2$ kW. It is seen for the case of simply having air in the holes of the MOF, that there is a continuous FWM-gain region extending from about 970 nm to 1170 nm. This means that we expect a somewhat continuous output spectrum in this wavelength region due to having anomalous dispersion at the pump wavelength [8].

When filled with water or methanol, the MOF shifts from having anomalous to normal dispersion at the pump wavelength (Fig. 1, right). One advantage of using FWM in the normal-dispersion regime as the sensing principle, is that the location and width of the FWM-peaks (determined by the wavelength range fulfilling $|\kappa(\lambda)| < 2\gamma P_0$) is almost independent of the amount of power coupled into the waveguide. This is seen in Fig. 2, right, from the steepness of the phase-mismatch curves for water and methanol through the wavelength region with

gain, indicated by horizontal dash-dotted lines. Changing the amount of power coupled into the waveguide would shift the position of the horizontal lines, but the high steepness of κ around 650–720 nm for water and methanol leads to an insignificant change in the gain region. In particular, for the case of water in the holes, we calculated that the anti-Stokes peak only shifts by about 2 nm, when increasing P_0 from 2.2 kW to 11 kW.

From the phase-match plot (Fig. 2, right) we predict the anti-Stokes peak to be located at ∼705 nm when there is water in the holes, and at ∼667 nm when there is methanol in the holes. Phase-matching on the long-wavelength side of the pump, i.e. the Stokes peak, (not shown in Fig. 2, right) occurs at ∼2160 nm for water and at ∼2630 nm for methanol.

3. Results

3.1. Simulations

The propagation of the pulses in the MOF were simulated using the generalized nonlinear Schrödinger equation [14, 28, 29]:

$$\frac{\partial \tilde{C}}{\partial z} - i\{\beta(\omega) - \beta(\omega_0) - \beta_1(\omega_0)[\omega - \omega_0]\}\tilde{C}(z,\omega) + \frac{\alpha(\omega)}{2}\tilde{C}(z,\omega) =$$
$$i\gamma(\omega)\left[1 + \frac{\omega - \omega_0}{\omega_0}\right]\mathscr{F}\left\{C(z,t)\int_{-\infty}^{\infty} R(T')\left|C(z,T-T')\right|^2 dT'\right\}, \quad (6)$$

where C is related to the Fourier transform $\tilde{A}(z,\omega) = \mathscr{F}\{A(z,t)\}$ of the field envelope $A(z,t)$ by [30]

$$\mathscr{F}\{C(z,t)\} = \tilde{C}(z,\omega) = \left[\frac{A_{\text{eff}}(\omega)}{A_{\text{eff}}(\omega_0)}\right]^{-1/4}\tilde{A}(z,\omega), \quad (7)$$

where $A_{\text{eff}}(\omega)$ is the frequency dependent effective mode area, and the nonlinear coefficient $\gamma(\omega)$ is given by [30]

$$\gamma(\omega) = \frac{n_2 n_0 \omega_0}{c n_{\text{eff}}(\omega)\sqrt{A_{\text{eff}}(\omega)A_{\text{eff}}(\omega_0)}}, \quad (8)$$

where n_2 is the nonlinear-index coefficient of the waveguide material set to the value corresponding to fused silica: $n_2 = 2.6 \cdot 10^{-20}$ m^2/W [14]. $n_{\text{eff}}(\omega)$ is the frequency dependent effective index of the guided mode and $n_0 = n_{\text{eff}}(\omega_0)$. The variation of $n_{\text{eff}}(\omega)$ is usually much smaller than the variation of $A_{\text{eff}}(\omega)$ and therefore neglected in the calculation of $\gamma(\omega)$. ω_0 is a chosen reference (angular) frequency and the center of the spectral simulation window. To obtain a suitable spectral window we chose ω_0 corresponding to a wavelength of 700 nm. $R(t)$ is the Raman response of the nonlinear waveguide. Here the standard approximation for silica glass was used [14, 31]:

$$R(t) = (1 - f_{\text{R}})\delta(t) + f_{\text{R}}\frac{\tau_1^2 + \tau_2^2}{\tau_1\tau_2^2}\exp(-t/\tau_2)\sin(t/\tau_1)\Theta(t), \quad (9)$$

where $\delta(t)$ is the Dirac delta function, $f_{\text{R}} = 0.18$ is the fractional Raman response, $\tau_1 = 12.2$ fs, $\tau_2 = 32$ fs, and $\Theta(t)$ is the Heaviside step function. Finally, $\alpha(\omega)$ is the wavelength dependent loss; since we found in Section 2.3 that the Stokes peaks with liquid in the holes should be located above 2000 nm, we included the so-called multiphonon edge loss of silica described by $\alpha(\lambda) = A\exp(-a/\lambda)$ (see Fig. 4 in Ref. [32]). We find that the higher loss experienced by the Stokes wave in the near-infrared does not significantly reduce the growth of the anti-Stokes wave in the visible, in accordance with previous findings [33]. The optical losses of the liquids are neglected, since the field overlap with the liquid compared to the overlap with
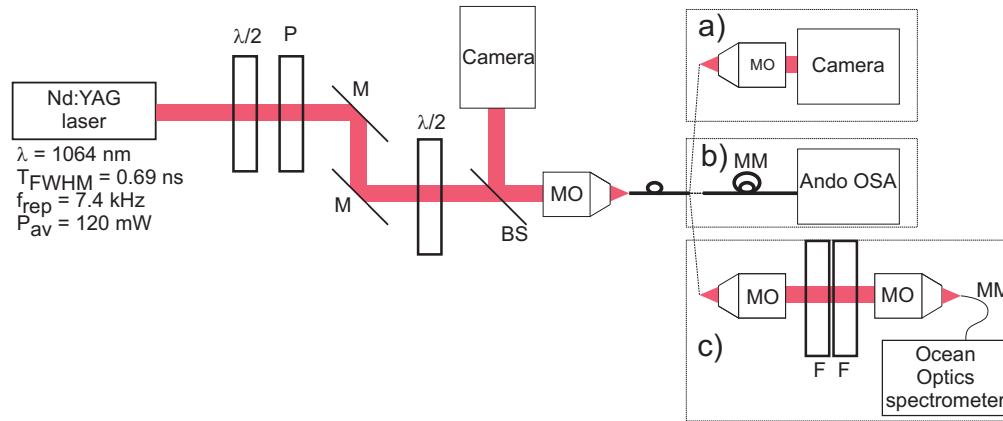
Fig. 3. Sketch of the experimental setup, with three different configurations for the output end of the fiber. $\lambda/2$: half-wave plate, P: polarizer, M: mirror, BS: beam splitter, MO: 20x microscope objective, MM: multimode fiber, F: filters reflecting 98–99% at 1064 nm, Ando OSA: AQ6315 optical spectrum analyzer, Ocean Optics spectrometer: HR2000+.

the silica glass is much smaller, and because of the relatively short propagation lengths used here. Equation (6) is solved using the interaction picture method [29, 34]. Both the frequency dependent propagation constant $\beta(\omega)$ and A_{eff} were calculated using the mode solving method described in Section 2.1.

It is well-known that FWM can grow from either input pump noise and/or quantum noise, and it is therefore important to choose a proper noise model for the simulations. We here used the combined phase-noise and one-photon-per-mode noise model, which was recently found to give good agreement with experimental measurements under highly different experimental conditions [35]. The 3-dB linewidth of the pump was set to 20 GHz (~ 0.08 nm). The simulation time window was 108 ps wide when simulating air or water in the holes, and 102 ps wide when simulating methanol in the holes (a slightly smaller temporal spacing was used in the latter case to obtain a frequency window broad enough to cover the Stokes peak at 2630 nm). Since the input pulses are experimentally 690 ps (FWHM) wide, we are essentially approximating the input as quasi-CW instead of including the full width of the pulses; this approach has previously been found to give good correspondence with experimental measurements while requiring fewer computational resources [35]. The input peak power was set to 2.2 kW, corresponding to a coupling efficiency of $\sim 20\%$ of the laser power, when including the 50% loss at the beam splitter used in the setup. Experimentally we found a coupling efficiency of $\sim 25\%$.

The results of the numerical simulations are shown in Figs. 4 and 5, where they are compared with the experimental measurements described in the following section.

3.2. Experiments

A sketch of the experimental setup is shown in Fig. 3. The pump laser is a compact diode pumped passively Q-switched Nd:YAG microchip laser from Teem Photonics, model SNP-13E, with specifications given in the figure. A half-wave plate and a polarizer, both rotatable, were used for simultaneous variable attenuation and optimization of the linear polarization for maximum reflection on the mirrors used to steer the beam height and direction. A second half-wave plate was used to control the polarization before the beam is coupled into the fiber using a microscope objective. A beam splitter and a camera were used as an aid in coupling the beam into the fiber core while controlling the X-Y-Z position of the fiber on a fiber stage.
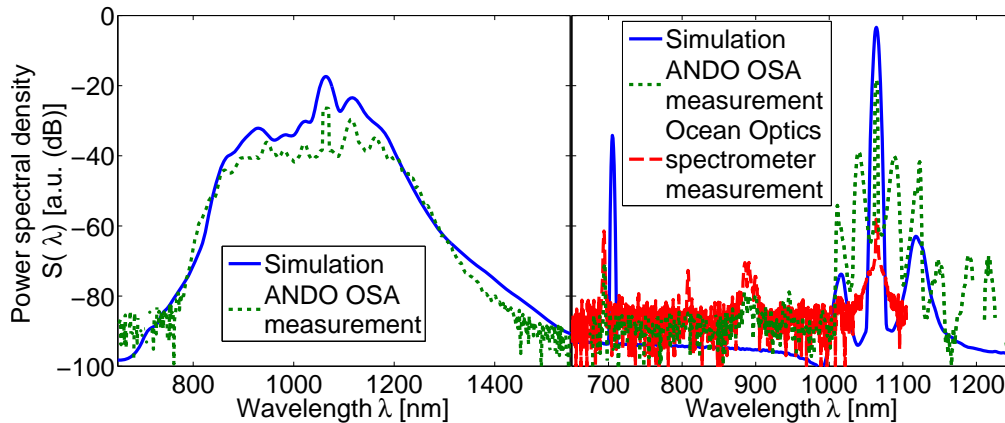
Fig. 4. *Left:* Simulation (blue, solid) and measurement (green, dotted) when using a 0.6 m long fiber without any liquid in the holes. The simulations are smoothed by convolution with a Gaussian function to ∼ 10 nm resolution. *Right:* Simulation (blue, solid) and measurement using either the ANDO OSA (green, dotted) or the Ocean Optics spectrometer (red, dashed) when using a 1.5 m long fiber with water in the holes. The simulations are smoothed by convolution to ∼ 2 nm resolution. Both simulated and measured spectra are vertically offset arbitrarily to qualitatively compare the simulations with the measurements. Note that two filters were used to attenuate near-infrared light (∼ 990–1140 nm) for measurements using the Ocean Optics spectrometer, to avoid saturation by the pump.

To ensure light was guided in the core, the output end of the fiber was also imaged with the camera (configuration a in Fig. 3). The output spectrum could be measured in two different configurations. In one, (configuration b in Fig. 3) we coupled the light from the nonlinear fiber into a multimode fiber connected to an ANDO OSA covering 350–1750 nm. With methanol in the holes it was difficult to measure the anti-Stokes signal in configuration b, so we also used configuration c in Fig. 3, where the output light from the nonlinear fiber is first collimated, then filtered to reduce the strong pump residual, before coupling the light into a multimode fiber connected to an Ocean Optics HR2000+ spectrometer covering 200–1100 nm. It was easier to find the anti-Stokes signal using the Ocean Optics HR2000+ due to its high sensitivity and fast measurement time (so that the coupling could be optimized while monitoring the spectrum), at the disadvantage of a lower dynamic range requiring the attenuation of the pump residual.

The liquids were filled into the air-holes of the MOF by using a pressure chamber with 5 bar overpressure for a few hours. The fiber ends were inspected in a microscope to verify that the liquid was filled all the way through the fiber. The fiber ends could ideally be sealed to contain the liquid, but since liquid leakage and evaporation from the fiber under atmospheric pressure and room temperature is very slow compared to the measurement time, we left the fiber ends unsealed. This could over time lead to some formation of air-bubbles in the holes, but as shown in the following this was not significant enough to hinder the observation of the anti-Stokes peaks. Besides keeping the procedure simple, the avoidance of sealing the ends also means that the same fiber could potentially be flushed with dry air after completing one measurement and reused with a different liquid. The water used for the experiments was purified and de-ionized (Milli-Q water), and the used methanol was specified to ≥ 99.9% purity.

Both simulated and measured spectra with only air in the holes are shown in Fig. 4, left. As expected in Section 2.3, pumping the fiber in the anomalous dispersion regime leads to a broad and continuous spectral broadening around the pump. A good qualitative agreement is seen between the simulation and the measurement.

We now consider the case with water in the holes, so the fiber is now pumped in the normal dispersion regime, which is expected to lead to narrow FWM peaks widely separated from the pump (cf. Section 2.3). As shown in Fig. 4, right, this is indeed the case for both the simulations and the measurements. First, both simulations and measurements show two peaks at ∼1120 nm and ∼1015 nm, which corresponds well with a 13 THz shift from the pump; this is the frequency shift at which the Raman effect in silica has maximum gain [14]. In standard silica fibers one would normally expect only to observe the Raman Stokes peak (∼1120 nm), but as pointed out by Coen *et al.* it is possible to also observe the Raman anti-Stokes peak (∼1015 nm) in MOFs due to the higher nonlinearity [36]. Two peaks at ∼1089 nm and ∼1040 nm are observed experimentally, but not in the simulations. Possible explanations for these peaks could be polarization dependent FWM [36] not included in the simulations, or a gradual partial evaporation of water from the holes and/or presence of air-bubbles in the holes, so that phase-matching corresponding to having air in the holes becomes possible at some length along the fiber; however these peaks are not of interest for this study and their origin therefore not investigated in more detail here. Some weak peaks are seen at 808 nm and ∼870–900 nm; control measurements using low pump power also showed these spectral features (Fig. 5, left, red dashed curve), so they must originate from the pump laser and are not due to any nonlinear effects in the fiber. The weak peak centered at 1148 nm (corresponding to a shift of 688 cm^{-1} from the pump) could be due to the L$_2$ Raman band of water at ∼680 cm^{-1} [37]. The weak peak at ∼1215 nm is shifted ∼700 cm^{-1} from the peak at ∼1120 nm, and could therefore be due to cascaded Raman scattering: first in the silica, then in the water. There is also a weak peak at ∼1190 nm which we have not been able to suggest the origin of, and it could therefore be due to another nonlinear effect, but not considered further here because of its irrelevance for the FWM anti-Stokes peak. Finally, we also observe a peak at 694 nm, only 11 nm from the theoretically predicted anti-Stokes peak at 705 nm. The fast response of the HR2000+ spectrometer allowed us to determine that the location of the anti-Stokes peak was insensitive to varying coupling conditions (both varying input beam position and power coupled into the fiber), only the strength of the peak changed. Note that the measurements using the HR2000+ spectrometer (red dashed curve in Fig. 4, right) were made using two filters before coupling into the spectrometer, which is why the peaks close to the pump are not seen in this configuration; the filters each had a peak reflectivity of ∼98–99% at 1064 nm with a 3-dB bandwidth of ∼150 nm.

Simulations and measurements when the holes of the fiber are filled with methanol are shown in Fig. 5, left. The Raman Stokes and anti-Stokes peaks are seen again in the simulations (blue, solid graph) at ∼1120 nm and ∼1015 nm, but not in the measurements (green, dotted graph) due to the use of the filters to avoid saturation by the pump. The peaks at 808 nm and ∼870–900 nm, previously determined to originate from the pump laser, are also seen. An additional peak is seen at 788 nm along with a broad peak around 750 nm; these are not expected from the simulations, but as for the case with water they could be due to polarization dependent FWM or gradual partial evaporation of methanol from the holes. We have also considered whether these peaks could be Raman anti-Stokes peaks for methanol, but the closest Raman frequencies for methanol are at 3330 cm^{-1} (very weak, broad) and 2940 cm^{-1} (very strong) [38], corresponding to 786 nm and 810 nm, respectively, for at pump at 1064 nm; it therefore seems unlikely that these peaks are due to Raman scattering in the methanol. Finally, a peak at 666 nm is observed experimentally, only 1 nm from the theoretically predicted anti-Stokes peak at 667 nm. This excellent agreement between theory and experiment is noteworthy, considering that this requires accurate calculation of the waveguide propagation constant $\beta(\omega)$ [Eq. (1)] at both the pump, Stokes, and anti-Stokes frequencies, the latter two being spaced apart almost 2000 nm, or more than two octaves.

A closer comparison of both the simulated and measured anti-Stokes peaks is shown in Fig. 5,
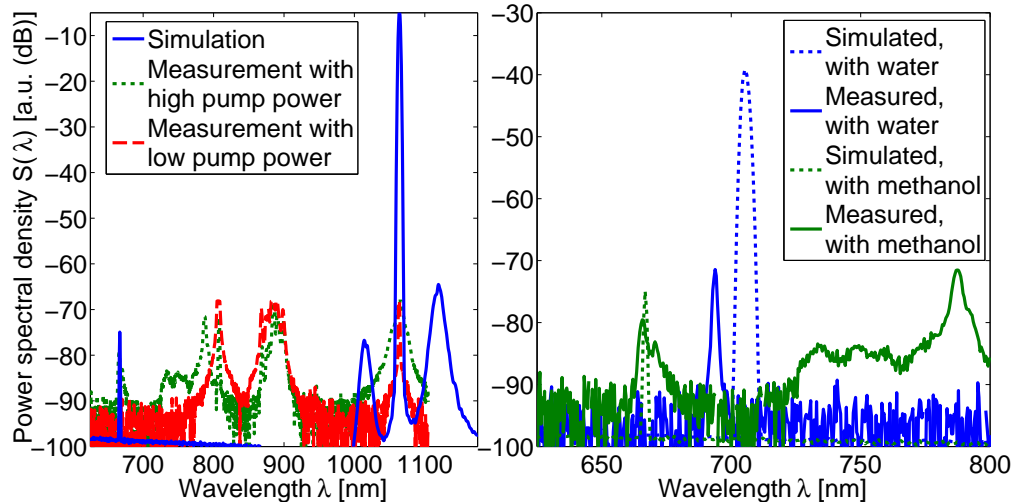
Fig. 5. *Left:* Simulation (blue, solid) and measurement (green, dotted) when pumping a 1.5 m long fiber with methanol in the holes. The simulations are smoothed by convolution to ~1 nm resolution. Measurements using low pump power are also shown (red, dashed) to identify spectral signatures originating from the pump laser itself without any significant nonlinear effects in the fiber. Note that the measured spectral power *level* using either high or low pump power is shown in a.u. and cannot be directly compared: in both cases the integration time and coupling into the spectrometer was adjusted to obtain higher signal-to-noise ratio without saturating the detector. *Right:* Comparison of simulations (dotted) and measurements (solid) using either water (blue) or methanol (green) in the holes of the fibre. All measurements for this figure were made using the Ocean Optics HR2000+, and two filters were used to attenuate light at ~990–1140 nm to avoid saturation by the pump.

right, for both water and methanol in the holes of the MOF. The measurements show that the anti-Stokes peak is shifted 28 nm further away from the pump with methanol in the holes, than with water.

4. Discussion

The 11 nm difference between calculated and measured anti-Stokes peak for the water-filled MOF could be caused by deviations between the modeled and actual microstructure of the MOF. However, we would expect structural deviations like this to lead to a larger difference between theory and experiment for the methanol-filled MOF, because the mode diameter (or A_{eff}) in this case is larger than in the water-filled MOF, and it would therefore be more sensitive to structural deviations. The difference could also be related to the influence of temperature on the refractive index of the investigated liquids, but we note that the data used for the calculations are valid at 25°C for both liquids [21,23], and the temperature derivative of the refractive index, $\mathrm{d}n/\mathrm{d}T$, is about 4 times higher for methanol than water [19]; the influence of temperature should therefore lead to a larger deviation between calculated and measured anti-Stokes peak for methanol, which is not the case.

We note that a previous liquid refractive index sensor based on long period gratings in a MOF was reported to have a sensitivity of $1.5 \cdot 10^3$ nm/Refractive Index Units (RIU) [39]. From our measurements, we find a sensitivity of $28 \text{ nm}/0.0032 \approx 8.8 \cdot 10^3$ nm/RIU, when considering the refractive index difference between water and methanol at the pump wavelength, even though we are simultaneously also probing n at the Stokes and anti-Stokes wavelengths.

It should be noted that this ubiquitously used definition of sensitivity should be used with care, since it implies a linear change in wavelength with refractive index, which is most likely not the case for our sensing principle. Still, the estimated sensitivity of $8.8 \cdot 10^3$ nm/RIU, indicates to an optical designer that using, e.g., an Ocean Optics HR2000+ spectrometer with a grating yielding a 0.5 nm resolution would ideally result in a minimally detectable change of 0.5 nm/$[8.8 \cdot 10^3$ nm/RIU$] = 6 \cdot 10^{-5}$ RIU. Choosing instead a grating with smaller spectral range but higher spectral resolution of 0.05 nm would instead result in a minimally detectable change of about $6 \cdot 10^{-6}$ RIU. We also note that we have used a commercially available fiber, and not just considered a MOF with a structure theoretically optimized for maximum sensitivity; it is therefore very likely that the sensitivity can be improved by using a MOF with a microstructure closer to an optimum design [9]. The highest experimentally demonstrated sensitivity for a fiber device to date is $30 \cdot 10^3$ nm/RIU, but that sensing principle was limited to be used only for liquids with n higher than the waveguide material [40]; one would therefore have to use e.g. special fluorinated polymers for the waveguide material to analyze aqueous solutions with $n \sim 1.33$, and these special polymers are not currently available for microstructured fibers. An alternative using high-index coated holes in a silica MOF was theoretically found to allow analysis of aqueous solutions, but at the expense of lowering the expected sensitivity down to $\sim 6.4 \cdot 10^3$ nm/RIU [41]. Another refractive index sensing scheme based on a solid twin-core MOF with a single liquid channel was recently suggested and found theoretically to have a sensitivity of ideally $70 \cdot 10^3$ nm/RIU [42]. In practice, this extremely high sensitivity is likely to be reduced due to e.g. micro- and macrobending losses, and fiber fabrication is not straightforward due to the necessity of drawing a preform consisting of two polymers having different mechanical properties. In contrast, the method demonstrated here relies only on already commercially available components and required no postprocessing of the fiber, except the simple process of filling all the holes of the fiber (selectively filling only one hole is not required).

One clever aspect of our sensing principle is that one could in principle even have the exact same refractive index of two different liquids at the pump wavelength, and still measure a shift in the FWM peaks as long as there is sufficient refractive index difference at e.g. the Stokes wavelength. In our case, the refractive index difference between the two liquids examined is actually 10 times larger at ~ 2400 nm than at 1064 nm, but it is still most relevant to define the sensitivity in terms of the refractive index difference at the pump wavelength. Another practical advantage of this approach for sensing is that one can use detectors in the visible to detect the location of the anti-Stokes peak, while actually also probing the refractive index at the Stokes peak located in the near-infrared. Using a detector sensitive in the near-infrared would, however, greatly increase the sensitivity when defined as wavelength-shift of the Stokes peak instead of the anti-Stokes peak, since the two peaks are equidistant from the pump in frequency, but the Stokes peak is further from the pump than the anti-Stokes peak, when measured in wavelength. Furthermore, we note the extreme simplicity of the sensing principle: no postprocessing of the fiber is required (e.g. grating writing as in Ref. [39]), nor does one have to selectively fill only one of the holes in the MOF with the analyte (as in Ref. [40]). In essence, only a pump laser and a spectrometer are required; use of a pressure chamber could potentially be avoided by using shorter fiber lengths and/or more patience, and letting capillary forces fill the fiber. For shorter fiber lengths it would, however, be necessary to investigate whether the FWM gain would allow the anti-Stokes peak to grow sufficiently above the detection noise floor. With postprocessing the refractive index sensor can be turned into a biosensor by adding a selective capture layer on the inside of the holes, using the technique described in Ref. [3].

The theoretical investigation in Ref. [9] estimated a shift in the anti-Stokes peak of 26 nm when a 5 nm biolayer was captured on the inside of the holes of an optimized MOF-structure, but it was unclear whether fluctuations in the MOF-structure along the fiber length would lower

the effective FWM-gain too much for a signal to be measured in practice. We used a non-optimized MOF-structure but still obtained a similar shift (28 nm) in the anti-Stokes peak when switching the MOF-filling liquid from water to methanol; this was even despite the fact that our anti-Stokes peak is located ∼30% further from the pump, and the decrease in effective FWM gain is expected to be more severe when trying to achieve phase-matching further from the pump [10]. Thus, our work also shows that the FWM-based sensing principle is robust in practice against fluctuations in the MOF-structure along the fiber length.

5. Conclusions

In conclusion, this is the first experimental work to demonstrate the feasibility of using four-wave mixing (FWM) as the sensing principle for a fiber optical refractive index sensor, and using liquid filling into the holes of a solid-core microstructured fiber to control the phase-match conditions for FWM. The principle is simple to realize experimentally: all components used are available commercially, and no complex postprocessing (e.g. grating writing or selective hole-filling) of the fiber is necessary. We obtained the highest sensitivity experimentally demonstrated to date for aqueous solutions ($n \sim 1.33$), which is relevant for extensions to biosensing, while optimization of the fiber microstructure is still possible for higher sensitivity.

Acknowledgments